Evaluation of the Grillo sensor, a low-cost accelerometer for IoT-based Real-time seismology

White paper

Vaclav Kuna[1,3], Diego Melgar[2,3], Andres Meira[3]

[1] *The Institute of Geophysics of the Czech Academy of Sciences, Prague, Czech Republic*
[2] *Department of Earth Sciences, University of Oregon, Eugene, Oregon, United States*
[3] *Grillo Holdings Inc., Cazenovia, NY, USA*

Micro-Electro-Mechanical systems (MEMS) accelerometers are useful for real-time seismology due to their ability to record strong, unsaturated seismic signals. Recent advances in MEMS technologies enable design of instruments with improved capabilities that also allow recording of small signals. As a result, MEMS can be useful across a broad dynamic range and for both major earthquakes and smaller magnitude events. Leveraging improved capabilities from off-the-shelf components, we demonstrate a new, low-cost MEMS-based accelerometer that provides an optimal tradeoff between instrument cost and performance. This article analyzes the instrument's performance in a regional network deployed in southern Mexico over a period of 3+ years for the purpose of earthquake early warning. We discuss the self-noise level, dynamic range, and useful resolution, and compare these parameters to other MEMS-based instruments. Besides the sensor evaluation, we present a large, openly available dataset of strong motion data that comprises continuous ground motion records from 24 instruments since 2017.

I. Introduction

Many regions of the world suffer from high earthquake-related risks due to a combination of growing population in hazard prone areas and fragile infrastructure that might not withstand strong ground shaking (Silva *et al.*, 2018). Earthquake Early Warning (EEW) systems can reduce these risks by providing users a short time window for taking a basic protective action before the strong shaking arrives. EEWs have proven to be capable of providing timely alerts during earthquakes in Mexico (Aranda *et al.*, 1995), Japan (Wenzel and Zschau, 2014), and Taiwan (Chen *et al.*, 2015). Multiple other EEW systems are either in development or undergoing testing (Allen and Melgar, 2019), such as on the US West coast (Kohler *et al.*, 2018), Italy (Satriano *et al.*, 2011), China (Jin *et al.*, 2013), or Israel (Nof and Kurzon, 2021).

There are two basic approaches to EEW systems. Regional or network-based EEW's make use of seismic networks located in, or near, a well-known seismic zone and aim to detect and characterize earthquakes a few seconds after their origin. Such systems exploit the difference between the fast electromagnetic communication of the system and the slower speed of seismic waves. Regional EEW's can provide useful alerts to sites farther than about 50 km from the earthquake epicenter. In contrast, on-site or single-station EEW's use the initial portion of the P-wave to predict the peak ground acceleration (often associated with slower S-wave) at that same site and are suitable for locations closer to the earthquake epicenter. Invariably, the choice of the type of system and algorithm depends strongly on available budgets. Sensor networks, including material cost and sensor deployment are one of the largest expenses in an EEW system and so the design of the system will be strongly controlled by how many stations can be afforded and what size

area the system needs to serve with that limited budget. For this reason, a low cost sensor that can be deployed in large numbers to provide dense station coverage across a large area has always been desirable.

Micro-electro-mechanical systems (MEMS) capacitive accelerometers offer this capability. They are low-cost, low-power sensors with a wide range of applications in multiple fields, such as electronics, engineering, and the military. Seismic applications have utilized MEMS sensors since the early 2000s (Holland, 2003). Their ability to record unsaturated, high-frequency, and especially near-field ground-motions (Evans et al., 2014), make them an economical choice for large-scale or dense seismic networks appropriate for EEW systems. MEMS instruments have been proven to be effective for regional EEW systems (Wu, 2015; Wu *et al.*, 2016; Peng *et al.*, 2019), on-site EEWs (Wu *et al.*, 2013, 2016), or used to densify existing networks of traditional, force-balance seismometers (Nof *et al.*, 2019). Kong *et al.* (2016) also designed a decentralized EEW based on crowdsourcing acceleration data from smartphone MEMS and Cochran *et al.* (2009) demonstrated using MEMS sensors in personal laptops.

In the past decade, scientists and engineers developed several MEMS-based instruments for EEW utilizing low-cost off-the-shelf components. Instruments such as Palert (Wu *et al.*, 2013), EDAS-MAS (Peng *et al.*, 2013), and Onavi (Cochran *et al.*, 2009) proved to be useful for recording high-amplitude ground motion. However, these kinds of sensors have relatively high self-noise, low resolution, and dynamic range, and as a result they fail to record small amplitude signals. Therefore, most of these rank among what is defined as a "Class-C" type instrument according to the Advanced National Seismic System (ANSS) categorization (USGS Open-File Report 2008-1262; Evans et al., 2014). This is a commonly accepted set of standards which classifies strong motion instruments based on their resolution and dynamic range. Other instruments, such as MAMA (Nof *et al.*, 2019), SOSEWIN (Fleming *et al.*, 2009), or GL-P2B (Peng *et al.*, 2017, 2019), have incorporated multiple analog MEMS sensors into a single device. In doing so, these instruments show improved data quality, allowing some of them to be ranked as ANSS Class B; however, the greater complexity of these devices might result in increased manufacturing costs.

MEMS technologies have continued to evolve and more recent advances have improved the quality of off-the-shelf components to the point that they now offer reduced self-noise and higher resolution than their ancestors. To leverage the capabilities of present-day components and maximize the performance of off-the-shelf MEMS sensors, Grillo, a social enterprise startup based in Mexico, has developed a new seismic instrument for EEW and other real-time seismology applications. The total cost of the components of the instrument that features a high-resolution, low-noise, low-power MEMS sensor is less than 100 USD.

The development of the new instrument is a part of a broader effort of developing a lightweight, low-cost EEW system based on the concept of the Internet of Things (IoT), that is, a system of mutually connected sensors and devices that exchange data over the internet. Using the IoT infrastructure, the Grillo instruments transmit real-time ground motion observations from sensors to cloud servers for detection, signal processing, and alert generation. Grillo has been testing the system in Mexico since 2017, where a seismic network located at the southeast coast of the country provides earthquake alerts to users in densely populated regions inland.

This article describes the design of the instrument and evaluates the sensor's performance in terms of self-noise, dynamic range, and useful resolution. We focus on both small amplitude signals such as P-waves as well as large amplitude ground motions. We discuss the sensor's reliability and compare its performance to other MEMS-based sensors developed for EEW applications. Finally, we also present a strong motion dataset collected during the 3-year deployment of 24 Grillo stations in a highly seismically active region in Mexico. We analyze signals of more than 700 earthquakes recorded at the network (including two major Mw > 7 events) and show that the Grillo instruments can, indeed, provide reliable information for rapid characterization of the earthquake source.

II. The Grillo seismic sensor

The sensor was designed with the primary goal of creating a reliable, high-performance, low-cost strong-motion sensor. The instrument consists of two major hardware components - the MEMS accelerometer module and the CPU module with Wifi and ethernet radios for data transmission.

The instrument uses the ADXL355 triaxial, low-noise, low-power MEMS accelerometer, with the selectable full-scale range of ±2, 4, or 8 g and an in-built 20-bit analog-to-digital (AD) converter. For the ±2 g option selected for the Grillo instrument, the sensor offers a resolution of ~4 μg/√Hz, which is roughly 1/5 of the sensor noise density of 22.5 μg/√Hz in the bandwidth of 0.095-1000 Hz (URL for the complete sensor specifications can be found in Data and Resources section). The sensor sampling rate can be configured to 31.25 or 125 Hz.

The Grillo instrument uses a Raspberry Pi 3b, this is a single-board computer with a 1.2 GHz 64-bit quad-core processor, with integrated Wi-Fi, Bluetooth, and Ethernet connectivity.

III. Grillo network and dataset

In late 2017, Grillo installed a network of 24 instruments along the Pacific coast in southwest Mexico to test the new strong-motion instrument and the overall feasibility of the IoT-based EEW system. This region of the country is highly seismically active due to the ongoing subduction of the Cocos plate underneath the North American Plate. This generated more than two dozen earthquakes larger than Mw 7.0 in the past 50 years (http://www.ssn.unam.mx/). The most destructive earthquake in modern times was the Mw 8.1 September 19, 1985, Michoacan event (Singh et al., 1988). Although 350 km from the earthquake rupture zone, the earthquake caused extensive damage and more than 20,000 casualties in Mexico City due to its setting on lakebed sediments that amplified the seismic waves and resonated at frequencies destructive for mid-rise buildings (Campillo *et al.*, 1989).

The EEW network (Fig. 1) consists of coastal sites located near the subduction front. It was designed to provide earthquake early warnings for the densely populated regions further inland in central Mexico, including Mexico City. The instruments are placed in schools, hospitals, and government buildings in the states of Guerrero (16 instruments), Oaxaca (6), Chiapas (1), and in Mexico City (1) (Fig. 1a). Each sensor is mounted on a primary structural element (e.g., concrete pillar) in the ground level of the building, with particular attention paid to searching for a quiet site. The sensors are leveled and connected by a power adapter and ethernet. They transmit live, 32 samples-per-second data streams to the Grillo platform on Amazon Web Services cloud via the MQTT protocol. Depending on the quality of internet connection, the data transmission latency is between 50 and 300 ms.

The network has recorded 722 events in the M 3.5-7.4 range (Fig. 1, 2) and the entire 1.1 TB dataset is openly available (see Data and Resources for details). The median data return from all stations until November 2017 is 81% (Fig. 1c). Data gaps are caused primarily by power and connectivity issues. Due to the lack of instrument maintenance in 2019, the data recovery drops from ~70% in 2018 to 50% in 2019 and increases to ~90% in 2020.

IV. Sensor performance

To evaluate the sensor's performance and its ability to record low-amplitude signals from small earthquakes, or large earthquakes occurring at a distance, we analyze the instrument's noise-level, dynamic range (DR), and useful resolution (NU).

We select 1-hour long instrument records (112500 samples) in three time periods in 2018, 2019, and 2020. These periods are chosen to maximize the number of live instruments in the three calendar years - all 24

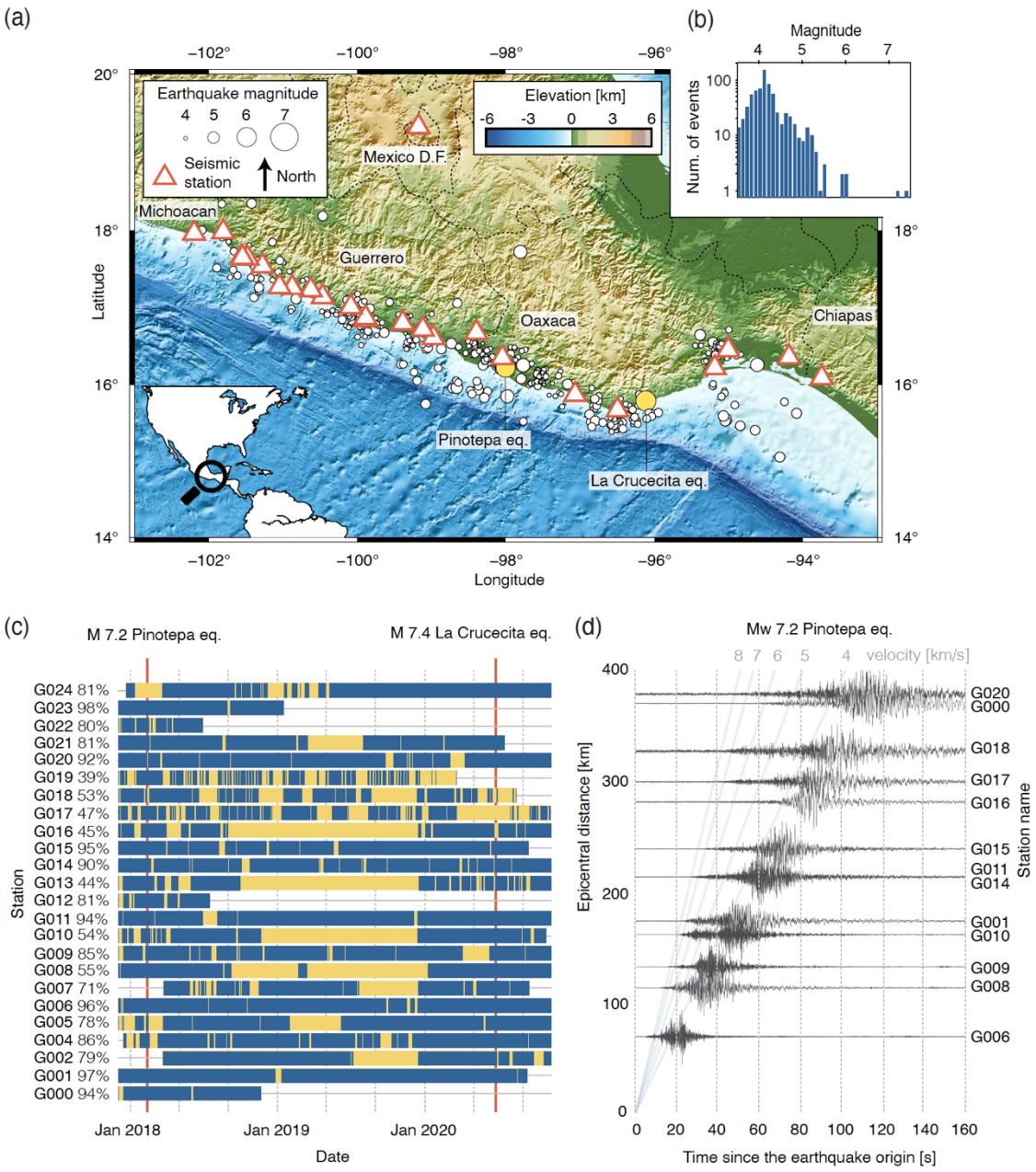

Figure 1. (a) Topographic map of southwest Mexico with locations of Grillo stations and earthquakes recorded by the network (see the main text for details). Epicenters of two major events (2018 Mw 7.2 Pinotepa and 2020 Mw 7.4 La Crucecita) are yellow. We use the GMRT global topographic grid (Ryan *et al.*, 2009). (b) Frequency-magnitude distribution of recorded events. (c) Station data recovery. The plot shows periods of continuous data recording (blue) and data gaps (yellow) between November 2017 and November 2020. The percentage shows the overall recovery rate at each station. Origin times of two major earthquakes are denoted with red lines. (d) Mw 7.2 Pinotepa earthquake recorded at the network (displayed up to the epicentral distance of 400 km).

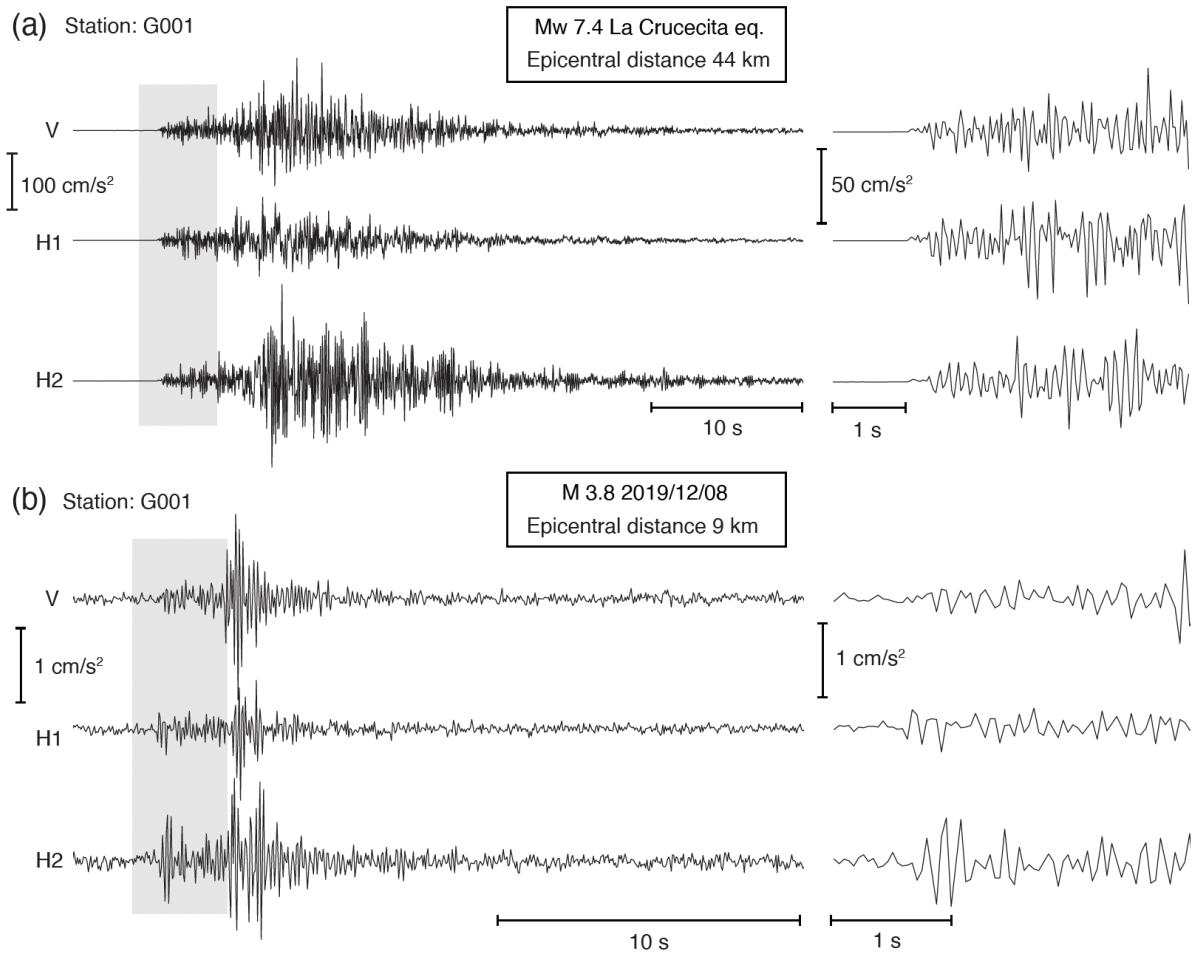

Figure 2. Example waveforms of (a) large (Mw 7.4 La Crucecita) and (b) small (M 3.8 on 2019/12/08) earthquakes recorded at G001. The left panel shows entire waveforms, the earthquake P-waves are amplified on the right.

instruments were live on July 6, 2018, 21:00-22:00, 19 on December 17, 2019, 17:00-18:00; and 18 on August 7, 2020, 1:00-2:00. We filter the data with a 4-pole Butterworth high-pass filter with a corner frequency of 0.01 Hz and ensure that the records do not contain any transient signals. For each instrument, we calculate the root mean square (RMS) of the vertical (V) and two horizontal (H1, H2) instrument components (Table 1). The RMS values are significantly higher than the ambient noise levels suggesting that the collected data represent the sensor's self-noise.

The RMS values are almost identical for the sensor's V and H1 component, averaging about 42 μg. The H2 component RMS is ~50% higher, which is due to differences in the construction of the individual components of the triaxial MEMS sensor. V and H1 are determined from capacitance between a set of movable plates along the flat dimension of the sensor; the H2 is measured by a single capacitor plate fixed on the torsion spring. The mean RMS values did not change significantly throughout the deployment, demonstrating the performance stability and reliability of the sensor. Following the definitions in Peng *et al.* (2019), we calculate the DR and NU using the mean RMS values and the full-scale seismometer range of ±2 g. For the V and H1 components, the DR averages over 90 dB; for H2, the DR is lower, with the mean value of 87 dB. The DR results in the useful resolution NU of 15 bits for V and H1 and 14.5 bits for H2.

We calculate the power spectral density (PSD) using the vertical components (Fig. 3). The PSD indicates an almost flat noise level of -77 dB (re 1 m/s^2) from 30 s to 10 Hz, with a gentle roll-off to -81 dB towards the Nyquist frequency (16 Hz). The PSD exceeds the microseismic high-noise model (HNM) in the entire frequency bandwidth, reaching roughly 20 dB higher than the HNM at the peak period of ~5 s. Comparison with representative earthquake spectral responses indicates that the sensor can detect peak accelerations of earthquakes with M > 2.5. at 10 km distance and M > 4.5 at 100 km distance (Clinton and Heaton, 2002).

We also compare the sensor performance against other MEMS-based accelerometers (Fig. 3a). The self-noise level is 25-50 dB lower than the self-noise of Class C MEMS sensors commonly used in consumer devices, such as smartphones (Kong *et al.*, 2016). It also performs better than instruments that use a single MEMS sensor, such as Onavi-B (Nof *et al.*, 2019). The performance of the Grillo instrument is similar to more complex MEMS-based accelerometers utilizing a series of sensors, such as MAMA (Nof *et al.*, 2019) and GL-P2B (Peng *et al.*, 2013). The sensor's overall performance, including the DR and the 20-bit AD converter resulting in the 4 μg resolution, rank the Grillo instrument into Class B of ANSS strong motion sensor classification.

V. Initial Observations and Results

Over the 3-year observation period, the network has recorded more than a thousand earthquakes. To show the instrument's capability for reliable recording of signals with a wide range of amplitudes, we analyze earthquake P-waves obtained by manual picking using the Pyrocko toolbox (Heimann *et al.*, 2017). Our network captured 722 earthquakes that allowed for reliable P-wave picking. For these events, we obtain earthquake source parameters (epicentral location, origin time, and magnitude) from the Mexican National Seismological Service (Servicio Sismológico Nacional; SSN) earthquake catalog. The Grillo network recorded earthquakes in the magnitude range between 3.5 and 7.4, recording 187 earthquakes of M<4; 478 of 4<M<5; 43 of 5<M< 6; 2 of 6<M< 7; 2 of M<7 (Fig. 1b). We were able to pick P-waves for M<4 earthquakes up to about 25 km away from the epicenter; the distance increases to 80 km for events 4<M<5 and 150 km for 5<M<6.

Earthquake magnitude in EEW is commonly estimated via the peak ground displacement (P_d) of the initial portion of the earthquake's P-wave (Li *et al.*, 2017; Trugman *et al.*, 2019). The decadic logarithm of P_d increases linearly with earthquake magnitude up to a magnitude of saturation. The magnitude of saturation depends on the length of the P-wave segment used for the calculation and can reach up to M 7.5 for roughly 10 s of initial P-wave (Trugman *et al.*, 2019). We calculated the P_d for 722 earthquakes (Fig. 1) using records

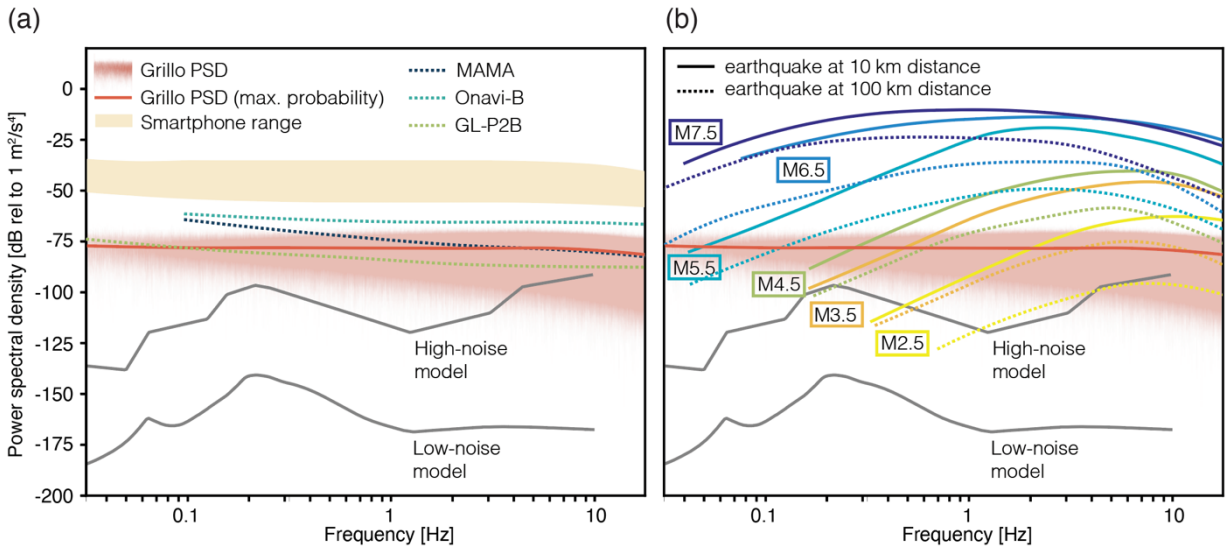

Figure 3. Grillo self-noise power spectral density (PSD) and its comparison with (a) other MEMS-based instruments and (b) typical seismic signals. PSD of Grillo sensors (light red area) was calculated using vertical components of 1-hour long records from all instruments (see text for details). The overall PSD of Grillo instruments (red line) was determined as the maximum probability PSD from the probability density function. Grey lines indicate low and high microseismic noise levels.

Table 1. Grillo instrument self-noise RMS, dynamic range (DR), and useful resolution (NU), calculated for all 3 sensor components in 3 time periods throughout the deployment (see text for details). The values give mean and standard deviation of values from individual instruments.

Self-noise (RMS), dynamic range (DR), and useful resolution (NU) of Grillo instruments

Period	**Vertical / V**			**Horizontal 1 / H1**			**Horizontal 2 / H2**		
1 hour (112500 samples)	**RMS** [μg]	**DR** [dB]	**NU** [bits]	**RMS** [μg]	**DR** [dB]	**NU** [bits]	**RMS** [μg]	**DR** [dB]	**NU** [bits]
June 2018	42.8 ± 2.0	90.4 ± 0.4	15.0 ± 0.1	42.0 ± 1.3	90.5 ± 0.3	15.0 ± 0.0	62.4 ± 4.1	87.1 ± 0.6	14.5 ± 0.1
December 2019	42.9 ± 2.0	90.4 ± 0.4	15.0 ± 0.1	42.0 ± 1.3	90.6 ± 0.3	15.0 ± 0.0	61.6 ± 2.5	87.2 ± 0.3	14.5 ± 0.1
August 2020	42.5 ± 1.5	90.4 ± 0.3	15.0 ± 0.1	41.0 ± 1.1	90.6 ± 0.2	15.0 ± 0.0	61.6 ± 2.4	87.2 ± 0.3	14.5 ± 0.1
Total	**42.7 ± 1.9**	**90.4 ± 0.4**	**15.0 ± 0.1**	**42.0 ± 1.2**	**90.6 ± 0.2**	**15.0 ± 0.0**	**61.9 ± 3.2**	**87.2 ± 0.4**	**14.5 ± 0.1**

filtered by the 4-pole Butterworth bandpass filter between 0.075 and 3 Hz (as used e.g. Li *et al.*, 2017; Trugman *et al.*, 2019). We use 1, 3, and 5 s long segments of the initial earthquake P-wave and correct the P_d to the common epicentral distance of 10 km. We observe a robust scaling of the P_d in the magnitude range between 3.5 and 6 for all lengths of the P-wave segments (Fig. 4). Earthquakes above this range also fit the predicted trend well. The P_d keeps increasing for earthquakes with M > 6 (especially for the M 7.4 La Crucecita earthquake) for all 1, 3, and 5 s long time windows, with no obvious sign of saturation. However, given that the data set is sparse for large events (only two earthquakes with M > 6), this result is not conclusive.

Two major earthquakes occurred during the period of observation. The first was the Mw 7.2 Pinotepa earthquake (UNAM Seismology Group, 2013, Li et al., 2018), which impacted the southwest coast of Oaxaca State on February 16, 2018. Maximum observed shaking intensities were VII on the Mercalli scale. The second was Mw 7.4 La Crucecita earthquake on June 23, 2020, with the epicenter located about 200 km southeast of the Pinotepa earthquake (Melgar et al., 2020; Villafuerte et al., 2020), which produced violent shaking of the maximum intensity of IX and caused widespread damage. The Grillo network recorded both earthquakes at 15 and 12 stations, respectively.

Using the observations of the Mw 7.2 Pinotepa and Mw 7.4 La Crucecita earthquake, we test the capability of the Grillo sensor to precisely capture high-amplitude ground motion accelerations (Fig. 5). We compare the observed peak ground acceleration (PGA) and the spectral acceleration (SA) with the regional ground motion model (GMM) of Arroyo *et al.*, 2010. The observed PGA attenuation rate is consistent with the prediction from the GMM for both earthquakes. The PGA residual mean of 0.57±0.36 suggests a slight but systematic underprediction of PGA by the GMM. The long-period ground motions represented in SA 3 s attenuate less rapidly than PGA, and the attenuation rate increases for SA 1.5 s and 0.5 s. The observed SA fit the predicted attenuation rates well, with almost all observations falling within the two sigma interval of the GMPE. The residuals suggest that there is no significant period or distance bias between the observations and the GMM predictions.

VI. Discussion and Conclusions

This article describes the development of a low-cost MEMS-based seismic instrument for EEW based on IoT. To test the instrument's performance, we set up a network of 24 instruments on the southwest Pacific coast of Mexico. All data since the deployment in late 2017 are openly available. We evaluated the sensor performance in terms of data recovery, self-noise level, dynamic range (DR), and useful resolution (NU). The DR exceeds 87 and 90 dB for individual components, which corresponds to NU of 15 and 14.5 bits. This ranks the instrument as an ANSS Class B type strong-motion sensor. The accelerometer can record peak accelerations of a local ~M 2.5 earthquake and has recorded more than 700 earthquakes with clear P-wave onsets. The P-wave peak ground displacement is a reliable predictor of earthquake magnitude in the entire magnitude range. The observed values of PGA and SA of 2 major earthquakes are in good agreement with GMM predictions, showing that the sensor provides reliable records over a wide range of signal amplitudes. Thus, the Grillo accelerometer meets the criteria for a reliable, low-cost strong-motion instrument.

In August 2020, Grillo launched OpenEEW (https://openeew.com/), an open-source initiative to share data, sensor technology, and detection algorithms, as a Code and Response with The Linux Foundation project. The OpenEEW enables collaborative development of the IoT-based EEW system, which focuses primarily on improving the seismic instrument, seismological algorithms, and development of the cloud platform. OpenEEW also allows free and unrestricted use of the EEW technology and any archived data, encouraging use of the system in earthquake-prone countries around the globe.

The OpenEEW community has now developed the second generation of the instrument, the OpenEEW sensor (Fig. 6) that differs from the Grillo sensor described here primarily in the choice of the CPU. It

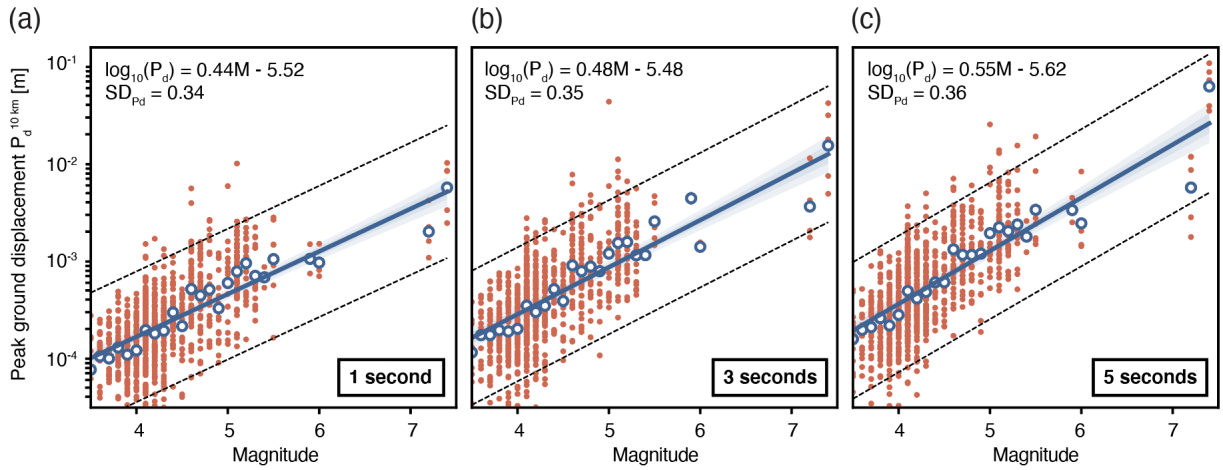

Figure 4. Peak ground displacement (P_d) vs. earthquake magnitude (M) using (a) 1 s, (b) 3 s, and (c) 5 s segment of initial earthquake P-wave. P_d is normalized to the common epicentral distance of 10 km, assuming the constant C to be equal to 1. The M-P_d relationship is determined by linear regression (blue line) and plotted together with the 95% uncertainty interval. Dashed lines represent a 95% interval of residuals ($P_{d\,OBS}$ - $P_{d\,PRED}$).

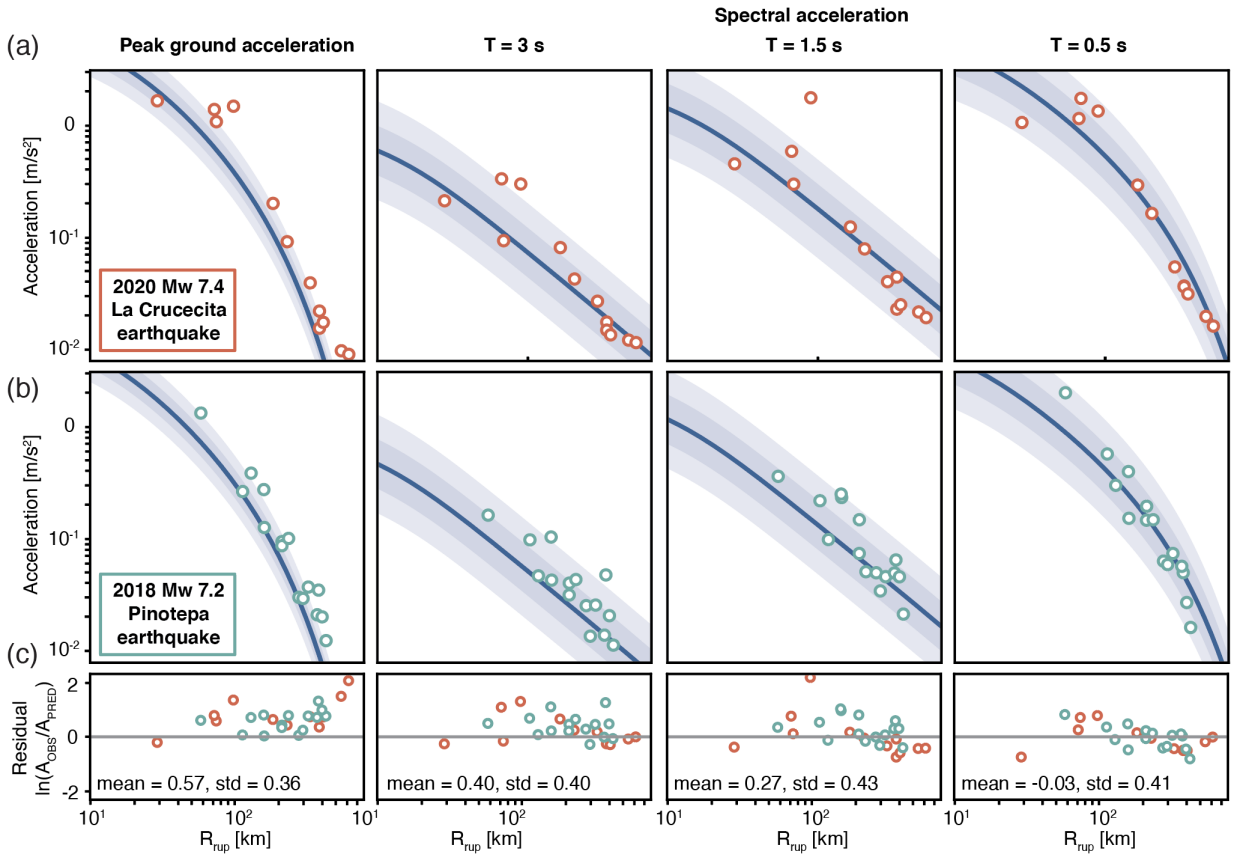

Figure 5. Comparison of observed and predicted peak ground accelerations (PGA) and spectral accelerations (SA) for (a) 2020 Mw 7.4 La Crucecita and (b) 2018 Mw 7.2 Pinotepa earthquake. SA is computed for periods of 3, 1.5. and 0.5 s. The predicted curves are calculated using GMPE inferred from intermediate and large earthquakes in Mexico (Arroyo *et al.*, 2010). 1 and 2 sigma intervals are plotted with shaded blue. (c) Residuals of PGA and SA calculated from observed and predicted values as $\ln(A_{OBS}/A_{PRED})$.

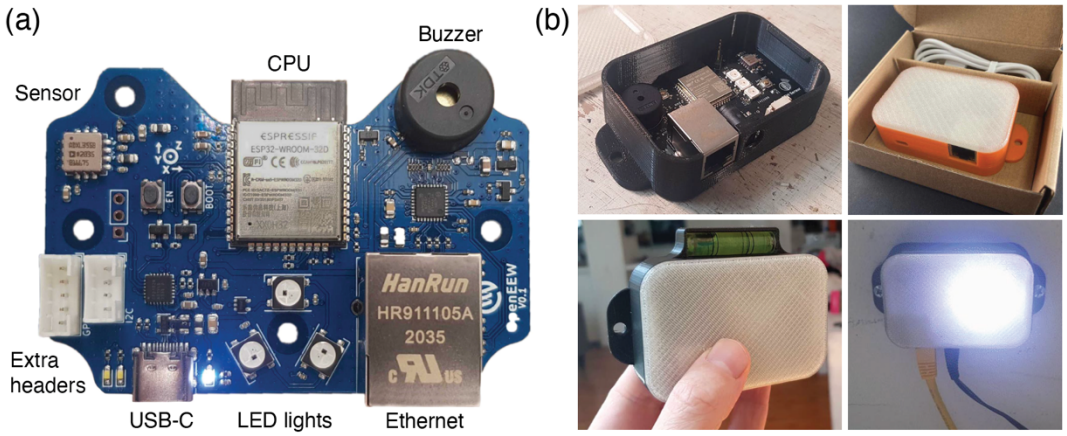

Figure 6. The OpenEEW seismic instrument. (a) The PCB containing all the instrument components. (b) Instrument packaging and deployment.

employs a low-cost, low-power ESP32 microcontroller with a dual-core Tensilica Xtensa LX6 microprocessor, which reduces the instrument cost and power consumption. It is contained in a custom-designed PCB board, with integrated Wi-Fi, Bluetooth, and Ethernet connectivity. Apart from that, it is equipped with RGB led lights and a buzzer that can be utilized for the EEW warning, and headers enabling the connection of a GPS module and various other sensors. The instrument works on an almost plug-and-play basis, with a very straightforward configuration through a smartphone app that passes the instrument's location and ID to the cloud. Thus, it can be easily installed and maintained by users with no technical background.

The simplicity of the instrument use may enable the general public to contribute to the EEW system by setting up personal instruments, improving the network density, limiting the maintenance costs, and securing the EEW sustainability. It may become an efficient solution for regional and on-site EEW's, or densifying the present networks of traditional force-balance instruments. A few projects based on OpenEEW are already planned or underway, such as in Puerto Rico and Nepal. All data collected during these experiments will be openly available as well.

VII. Data and Resources

All the data and codes used in this article are openly available. Grillo micro-electromechanical (MEMS) accelerometer data are available in JSON format at Amazon S3 storage under the bucket name grillo-openeew (https://s3.console.aws.amazon.com/s3/buckets/grillo-openeew). They can be downloaded through standard AWS S3 access mechanisms or via OpenEEW Python packages. The OpenEEW package for Python is available at https://github.com/openeew/openeew-python. OpenEEW sensor can be purchased at https://openeew.com. The ADXL355 sensor specifications can be accessed at https://www.analog.com/media/en/technical-documentation/data-sheets/adxl354_adxl355.pdf. The Servicio Sismológico Nacional (SSN) seismicity catalog was obtained at http://www2.ssn.unam.mx:8080/catalogo/. The observed and theoretical peak ground acceleration (PGA), spectral acceleration (SA) values were calculated using MudPy, which can be obtained at https://github.com/dmelgarm/mudpy. All websites were last accessed in November 2020. Some plots were made using the Generic Mapping Tools version 6 (generic-mapping-tools.org; Wessel et al., 2019).

VIII. Acknowledgments

The development of the instruments was supported by USAID, IBM, Linux Foundation, Roddenbury Foundation, Arrow Electronics, and Clinton Global Initiative. We thank the OpenEEW community that contributes to the development of the EEW. We also thank Michael Allman, Allen Husker, and Luis Rodriguez for their help in designing the sensor, cloud architecture, and deploying the network. SSN data products, station maintenance, data acquisition and distribution are thanks to its personnel.

IX. Competing interests

Authors hold equity in Grillo Inc..

X. References

Allen, R. M., and D. Melgar (2019). Earthquake Early Warning: Advances, Scientific Challenges, and Societal Needs, *Annu. Rev. Earth Planet. Sci.* **47**, no. 1, 361–388, doi: 10.1146/annurev-earth-053018-060457.

Aranda, J. M. E., A. Jimenez, G. Ibarrola, F. Alcantar, A. Aguilar, M. Inostroza, and S. Maldonado (1995). Mexico City Seismic Alert System, *Seismological Research Letters* **66**, no. 6, 42–53, doi: 10.1785/gssrl.66.6.42.

Arroyo, D., D. García, M. Ordaz, M. A. Mora, and S. K. Singh (2010). Strong ground-motion relations for Mexican interplate earthquakes, *J Seismol* **14**, no. 4, 769–785, doi: 10.1007/s10950-010-9200-0.

Campillo, M., J. C. Gariel, K. Aki, and F. J. Sánchez-Sesma (1989). Destructive strong ground motion in Mexico city: Source, path, and site effects during great 1985 Michoacán earthquake, *Bulletin of the Seismological Society of America* **79**, no. 6, 1718–1735.

Chen, D., N. Hsiao, and Y. Wu (2015). The Earthworm Based Earthquake Alarm Reporting System in Taiwan, *Bulletin of the Seismological Society of America* **105**, no. 2A, 568–579, doi: 10.1785/0120140147.

Clinton, J. F., and T. H. Heaton (2002). Potential Advantages of a Strong-motion Velocity Meter over a Strong-motion Accelerometer, *Seismological Research Letters* **73**, no. 3, 332–342, doi: 10.1785/gssrl.73.3.332.

Cochran, E., J. Lawrence, C. Christensen, and A. Chung (2009). A novel strong-motion seismic network for community participation in earthquake monitoring, *IEEE Instrum. Meas. Mag.* **12**, no. 6, 8–15, doi: 10.1109/MIM.2009.5338255.

Cochran, E. S., J. F. Lawrence, C. Christensen, and R. S. Jakka (2009). The Quake-Catcher Network: Citizen Science Expanding Seismic Horizons, *Seismological Research Letters* **80**, no. 1, 26–30, doi: 10.1785/gssrl.80.1.26.

Evans, J., R. Allen, A. Chung, E. Cochran, R. Guy, M. Hellweg, and J. Lawrence (2014). Performance of Several Low-Cost Accelerometers, *Seismological Research Letters* **85**, 147–158, doi: 10.1785/0220130091.

Fleming, K., M. Picozzi, C. Milkereit, the S. and E. working Groups, F. Kühnlenz, the S. and E. working Groups, B. Lichtblau, the S. and E. working Groups, J. Fischer, the S. and E. working Groups, *et al.* (2009). The Self-organizing Seismic Early Warning Information Network (SOSEWIN), *Seismological Research Letters* **80**, no. 5, 755–771, doi: 10.1785/gssrl.80.5.755.

Heimann, S., M. Kriegerowski, M. Isken, S. Cesca, S. Daout, F. Grigoli, C. Juretzek, T. Megies, N. Nooshiri, A. Steinberg, *et al.* (2017). Pyrocko - An open-source seismology toolbox and library, doi: 10.5880/GFZ.2.1.2017.001.

Holland, A. (2003). Earthquake Data Recorded by the MEMS Accelerometer: Field Testing in Idaho, *Seismological Research Letters* **74**, no. 1, 20–26, doi: 10.1785/gssrl.74.1.20.

Jin, X., Y. Wei, J. Li, H. Zhang, Q. Ma, and L. Kang (2013). Progress of the earthquake early warning system in Fujian, China, *Earthquake Science* **26**, no. 1, 3–14.

Kohler, M. D., E. S. Cochran, D. Given, S. Guiwits, D. Neuhauser, I. Henson, R. Hartog, P. Bodin, V. Kress, S. Thompson, *et al.* (2018). Earthquake Early Warning ShakeAlert System: West Coast Wide Production Prototype, *Seismological Research Letters* **89**, no. 1, 99–107, doi: 10.1785/0220170140.

Kong, Q., R. M. Allen, L. Schreier, and Y.-W. Kwon (2016). MyShake: A smartphone seismic network for earthquake early warning and beyond, *Science Advances* **2**, no. 2, e1501055, doi: 10.1126/sciadv.1501055.

Li, H., J. Zhang, and Y. Tang (2017). Testing Earthquake Early Warning Parameters, τpmax, τc, and Pd, for Rapid Magnitude Estimation in the Sichuan, China, RegionTesting Earthquake Early Warning Parameters for Rapid Magnitude Estimation in the Sichuan Region, *Bulletin of the Seismological Society of America* **107**, no. 3, 1439–1450, doi: 10.1785/0120160386.

Li, Y., X. Shan, C. Zhu, X. Qiao, L. Zhao, and C. Qu (2020). Geodetic Model of the 2018 Mw 7.2 Pinotepa, Mexico, Earthquake Inferred from InSAR and GPS Data, *Bulletin of the Seismological Society of America* **110**, no. 3, 1115–1124, doi: 10.1785/0120190101.

Melgar, D., A. Ruiz-Angulo, X. Pérez-Campos, B. W. Crowell, X. Xu, E. Cabral-Cano, M. R. Brudzinski, and L. Rodriguez-Abreu (n.d.). Energetic Rupture and Tsunamigenesis during the 2020 Mw 7.4 La Crucecita, Mexico Earthquake, Seismological Research Letters, doi: 10.1785/0220200272.

Nof, R. N., A. I. Chung, H. Rademacher, L. Dengler, and R. M. Allen (2019). MEMS Accelerometer Mini-Array (MAMA): A Low-Cost Implementation for Earthquake Early Warning Enhancement, *Earthquake Spectra* **35**, no. 1, 21–38, doi: 10.1193/021218EQS036M.

USGS Open-File Report 2008-1262: Instrumentation Guidelines for the Advanced National Seismic System (n.d.): <https://pubs.usgs.gov/of/2008/1262/> (accessed December 4, 2020).

Ometepec-Pinotepa Nacional, Mexico Earthquake of 20 March 2012 (Mw 7.5): A preliminary report | Geofísica Internacional (n.d.): <https://www.elsevier.es/en-revista-geofisica-internacional-80-articulo-ometepec-pinotepa-nacional-mexico-earthquake-20-S0016716913714715> (accessed December 4, 2020).

Peng, C., Y. Chen, Q. Chen, J. Yang, H. Wang, X. Zhu, Z. Xu, and Y. Zheng (2017). A new type of tri-axial accelerometers with high dynamic range MEMS for earthquake early warning, *Computers & Geosciences* **100**, 179–187, doi: 10.1016/j.cageo.2017.01.001.

Peng, C., P. Jiang, Q. Chen, Q. Ma, and J. Yang (2019). Performance Evaluation of a Dense MEMS-Based Seismic Sensor Array Deployed in the Sichuan-Yunnan Border Region for Earthquake Early Warning, 11, *Micromachines* **10**, no. 11, 735, doi: 10.3390/mi10110735.

Peng, C., X. Zhu, J. Yang, B. Xue, and Y. Chen (2013). Development of an integrated on-site earthquake early warning system and test deployment in Zhaotong, China, *Computers & Geosciences* **56**, 170–177, doi: 10.1016/j.cageo.2013.03.018.

Ryan, W. B. F., S. M. Carbotte, J. O. Coplan, S. O'Hara, A. Melkonian, R. Arko, R. A. Weissel, V. Ferrini, A. Goodwillie, F. Nitsche, *et al.* (2009). Global Multi-Resolution Topography synthesis, *Geochem. Geophys. Geosyst.* **10**, Q03014, doi: 10.1029/2008GC002332.

Satriano, C., L. Elia, C. Martino, M. Lancieri, A. Zollo, and G. Iannaccone (2011). PRESTo, the earthquake early warning system for Southern Italy: Concepts, capabilities and future perspectives, *Soil Dynamics and Earthquake Engineering* **31**, no. 2, 137–153, doi: 10.1016/j.soildyn.2010.06.008.

Silva, V., D. Amo-Oduro, A. Calderon, J. Dabbeek, V. Despotaki, L. Martins, A. Rao, M. Simionato, D. Viganò, C. Yepes, *et al.* (2018). Global Earthquake Model (GEM) Seismic Risk Map (version 2018.1), doi: 10.13117/GEM-GLOBAL-SEISMIC-RISK-MAP-2018.1.

Singh, S. K., E. Mena, and R. Castro (1988). Some aspects of source characteristics of the 19 September 1985 Michoacan earthquake and ground motion amplification in and near Mexico City from strong motion data, Bulletin of the Seismological Society of America 78, no. 2, 451–477.

Trugman, D. T., M. T. Page, S. E. Minson, and E. S. Cochran (2019). Peak Ground Displacement Saturates Exactly When Expected: Implications for Earthquake Early Warning, *J. Geophys. Res. Solid Earth* **124**, no. 5, 4642–4653, doi: 10.1029/2018JB017093.

Villafuerte, C., V. M. Cruz-Atienza, J. Tago, D. Solano-Rojas, S. Franco, R. Garza-Girón, L. A. Dominguez, and V. Kostoglodov (2020). Slow slip events and megathrust coupling changes reveal the earthquake potential before the 2020 Mw 7.4 Huatulco, Mexico event, preprint, Earth and Space Science Open Archive: <http://www.essoar.org/doi/10.1002/essoar.10504796.3> (accessed December 4, 2020).

Wenzel, F., and J. Zschau (Editors) (2014). *Early Warning for Geological Disasters*, Springer Berlin Heidelberg, Berlin, Heidelberg, Advanced Technologies in Earth Sciences, doi: 10.1007/978-3-642-12233-0.

Wessel, P., Luis, J. F., Uieda, L., Scharroo, R., Wobbe, F., Smith, W. H. F., & Tian, D. (2019). The Generic Mapping Tools version 6. Geochemistry, Geophysics, Geosystems, 20, 5556–5564. https://doi.org/10.1029/2019GC008515

Wu, Y.-M. (2015). Progress on Development of an Earthquake Early Warning System Using Low-Cost Sensors, *Pure Appl. Geophys.* **172**, no. 9, 2343–2351, doi: 10.1007/s00024-014-0933-5.

Wu, Y.-M., D.-Y. Chen, T.-L. Lin, C.-Y. Hsieh, T.-L. Chin, W.-Y. Chang, W.-S. Li, and S.-H. Ker (2013). A High-Density Seismic Network for Earthquake Early Warning in Taiwan Based on Low Cost Sensors, *Seismological Research Letters* **84**, no. 6, 1048–1054, doi: 10.1785/0220130085.

Wu, Y.-M., W.-T. Liang, H. Mittal, W.-A. Chao, C.-H. Lin, B.-S. Huang, and C.-M. Lin (2016). Performance of a Low-Cost Earthquake Early Warning System (P-Alert) during the 2016 ML 6.4 Meinong (Taiwan) Earthquake, *Seismological Research Letters* **87**, no. 5, 1050–1059, doi: 10.1785/0220160058.

Nof, R. N., and I. Kurzon (2021). TRUAA—Earthquake Early Warning System for Israel: Implementation and Current Status. Seismological Society of America 92, no. 1, 325-341.